The Astrophysical Journal, 970:26 (8pp), 2024 July 20 https://doi.org/10.3847/1538-4357/ad5007

Millimeter to THz Spectroscopy of $HC^{18}O^+$ and $HC^{17}O^+$: Accurate Rest Frequencies for Astrophysical Studies

Luca Bizzocchi[1], Francesca Tonolo[1], Barbara M. Giuliano[2], Paola Caselli[2], Mattia Melosso[1], Luca Dore[1], Silvia Alessandrini[1], Cristina Puzzarini[1], and Andrea Pietropolli Charmet[3]
[1] Dipartimento di Chimica "Giacomo Ciamician," Università di Bologna, via F. Selmi 2, 40126 Bologna, Italy; luca.bizzocchi@unibo.it
[2] Center for Astrochemical Studies, Max-Planck-Institut für extraterrestrische Physik, Gießenbachstr. 1, 85748 Garching bei München, Germany
[3] Dipartimento di Scienze Molecolari e Nanosistemi, Università Ca' Foscari Venezia, via Torino 155, 30172 Mestre, Italy
Received 2024 March 25; revised 2024 May 14; accepted 2024 May 22; published 2024 July 12

Abstract

Heavy oxygen isotopic species of HCO^+ are important optically thin astrophysical tracers. The ground-state rotational spectrum of $HC^{18}O^+$, $DC^{18}O^+$, $HC^{17}O^+$, and $DC^{17}O^+$ has been recorded in the laboratory in the frequency range from 85 GHz to 1.3 THz. The ions have been produced in the negative column of a glow-discharge plasma, and their spectrum has been recorded in absorption using a frequency-modulation submillimeter-wave spectrometer. Various sources of systematic error have been carefully accounted for in order to obtain highly accurate line-position measurements. Theoretical estimates of the molecular parameters and of the collision effects on the line shape have been obtained by high-level ab initio calculations. The analysis yielded much improved rotational and centrifugal distortion constants, thus bringing the spectroscopic characterization of these rare isotopic variants to the same level of the parent species. Also, the first experimental rotational data for $DC^{17}O^+$ have been provided. These results allow for the calculation of an updated set of rest frequencies to support current and future astrophysical studies. The derived data set for the widely used $HC^{18}O^+$ tracer reaches an accuracy of a few parts in 10^9 up to 1.5 THz. Such accuracy is important for the analysis of astrophysical objects targeted by Atacama Large Millimeter/submillimeter Array observations at the submillimeter regime.

Unified Astronomy Thesaurus concepts: Laboratory astrophysics (2004); Spectral line lists (2082); Collisional broadening (2083)

1. Introduction

Formylium (HCO^+) was the first ionic species ever identified in space. Its fundamental $J = 1$–0 transition was observed by Buhl & Snyder (1970) and remained unassigned for a while (labeled as X-ogen; see Herbst & Klemperer 1974) until its rotational spectrum was finally recorded in the laboratory (Woods et al. 1975). This ion has CO as parent molecules—the most abundant species in the interstellar medium (ISM) after H_2—and its main formation route involves proton transfer from H_3^+, which is produced by cosmic-ray ionization. Due to its simple formation chemistry and the abundance of the precursors, HCO^+ is ubiquitous in space and is readily observed in a multitude of sources representing all the phases of ISM (see, e.g., Lattanzi et al. 2007 for a comprehensive list of examples), young and evolved stars (Qi et al. 2003; Agúndez & Cernicharo 2006), and comets (Milam et al. 2004), as well as in extragalactic objects up to a relatively large redshift (e.g., $z = 3.91$; Riechers et al. 2010).

HCO^+ is characterized by a large dipole moment ($\mu = 3.9$ D; Botschwina et al. 1993), and it is thus a specialized tracer of high-density regions. However, rotational transitions of HCO^+ often present high optical opacity, thus making the determination of molecular abundances from the observed fluxes cumbersome. One customary way to overcome this difficulty is to observe the thinner emissions originated from the corresponding lines of the less abundant isotopologues. However, as $H^{13}CO^+$(∼1%) is also optically thick in many sources, one has often to resort to species containing oxygen-heavy isotopes, such as $HC^{18}O^+$(∼0.2%) and $HC^{17}O^+$(∼0.04%). Since they trace the material throughout the cloud, such optically thin emitters also provide a means to accurately study the source gas dynamics (e.g., infall along the line of sight; Tafalla et al. 1998; Ferrer Asensio et al. 2022) or the depletion mechanisms at work in the denser parts of the core (Caselli et al. 2002). Rare isotopic variants of common tracers thus play a major diagnostic role, and their accurate spectroscopic characterization is a strategic requisite for a thoughtful interpretation of observational data.

Generally speaking, very accurate rest frequencies—ideally obtained directly by laboratory measurements—are required for any molecule targeted by radio-astronomical observation. More specifically, accuracies within a few parts per million are needed to extract reliable dynamical information from the observed emission profiles (e.g., Caselli & Dore 2005). Nowadays, most of the major astrophysical tracers have been thoroughly investigated in the laboratory, and their spectroscopic signatures are known with great precision (e.g., Cazzoli et al. 2003, 2004). Among them, HCO^+ is no exception, with recent studies providing reliable and highly accurate rest frequencies up to the THz regime (Lattanzi et al. 2007; Tinti et al. 2007; Cazzoli et al. 2012). While this is true, up to a certain extent, for $H^{13}CO^+$ and DCO^+ as well (e.g., Lattanzi et al. 2007), the situation is less satisfactory for the ^{18}O- and ^{17}O-bearing species, for which laboratory spectroscopic investigations have been much less extensive. Regarding $HC^{18}O^+$, only a few transitions were recorded in the laboratory: the $J = 3$–2 one by Plummer et al. (1983) and subsequently, a few more low-J transitions by Warner (1988;

reported by Puzzarini et al. 1996). Later on, the rest frequency of the $J = 1$–0 line was also obtained through radio-astronomical observations (Schmid-Burgk et al. 2004). The laboratory spectrum of the rarer $HC^{17}O^+$ isotopologue was studied by Dore et al. (2001a, 2001b) in the millimeter frequency range below 200 GHz, and a detailed analysis of the hyperfine structure (HFS) due to the ^{17}O-quadrupole coupling was also provided (Dore et al. 2001b).

Here, we present a new, comprehensive laboratory investigation of the $HC^{18}O^+$, $DC^{18}O^+$, $HC^{17}O^+$, and $DC^{17}O^+$ isotopologues. Our objective is to achieve a sound spectroscopic characterization of these rare yet astrophysically important formylium variants over the whole frequency range of interest to radio astronomy. Special attention has been paid to minimize various possible systematic errors affecting the experimental measurements, with the aim of improving, to the maximum extent, the accuracy of the derived rest frequencies. In detail, the line-shape distortion due to the unresolved HFS has been explicitly modeled for $HC^{17}O^+$, whereas the collisional shift has been precisely estimated by measurements and theoretical calculations to evaluate its impact on the low-J spectrum of $HC^{18}O^+$.

The paper is structured as follows: In Section 2 we briefly describe our experiments, and in Section 3 we give an account of the supporting theoretical calculations. In Section 4, details about the analysis of the laboratory data are provided; they include a description of the various sources of measurement uncertainty considered (Sections 4.2 and 4.3) and an account of the spectral fit carried out on the final "corrected" data set (Section 4.4). Finally, we discuss the results and draw our conclusions in Section 5.

2. Experimental Details

The rotational spectra of HCO^+ rare isotopologues have been observed in absorption using the CASAC spectrometer located at the Max-Planck-Institut für extraterrestrische Physik in Garching. A detailed description of the experimental apparatus is given elsewhere (Bizzocchi et al. 2017). Briefly, the instrument is a frequency-modulation (FM) millimeter spectrometer which employs a 3 mm band (82–125 GHz) active multiplier chain (AMC-WR9, Virginia Diodes) as a primary radiation source. Additional frequency multipliers provide operation up the THz regime with an available power of a few microwatts. A cryogenic-free, closed-cycle He-cooled InSb hot electron bolometer (QMC Instruments Ltd.) is used as a detector. FM is obtained by 50 kHz sine-wave modulation of the carrier frequency; phase-sensitive detection at $2f$ then delivers the second derivative of the actual absorption profile. The modulation depth is adjusted to match the spectral width of the target signals according to the experimental conditions.

Ions are produced by sustaining a direct current (DC) glow discharge in the absorption cell (a 3 m long, 5 cm in diameter Pyrex tube) that hosts two stainless steel, cylindrical, hollow electrodes separated by 2 m. Formylium has been produced in the negative column of the discharge by flowing a mixture of 3 mTorr (0.4 Pa) of CO, 1 mTorr of H_2 (0.13 Pa), and 15–20 mTorr (~3.3 Pa) of Ar as carrier gas. The plasma region is cooled at 85–100 K by liquid nitrogen circulation. In the typical discharge conditions, the current was kept in the 10–15 mA range with an applied voltage of ~2.5 kV. A ~250 G axial magnetic field has been applied coaxially to the plasma to improve the ion production in the extended negative column. Once optimal discharge conditions were achieved, the CO precursor was replaced with an ^{18}O-enriched sample (95%) to increase the abundance of formylium isotopic species. Such a sample contains ~1% of $C^{17}O$, so its use improves substantially the $HC^{17}O^+$ generation too. D_2 was used in place of H_2 to generate the deuterated variants ($DC^{18}O^+$ and $DC^{17}O^+$). In total, we measured 17 lines for $HC^{18}O^+$, from $J = 1$–0 to $J = 17$–16; 8 lines for $DC^{18}O^+$, from $J = 9$–8 to $J = 17$–16; 11 lines for $HC^{17}O^+$, from $J = 3$–2 to $J = 13$–12; and also 9 lines for $DC^{17}O^+$, from $J = 3$–2 to $J = 11$–10.

3. Theoretical Calculations

With the aim of estimating the effect of the plasma buffer gas on low-J transitions of formylium isotopologues, we have performed full close coupling scattering calculations for the $HC^{18}O^+$–Ar collisional system. Within the Born–Oppenheimer approximation, the interaction potential is independent from the choice of the isotopologue for either the target or the collider species. What actually affects the collision dynamics is the variation of the Jacobi coordinates due to the displacement of the center of mass of the system. This enables concentrating the effort on the calculation of the potential for the parent HCO^+–Ar system, which is then easier to validate through comparison with experimental data (e.g., Tonolo et al. 2022).

The interaction energies between HCO^+ and Ar have been computed at the CCSD(T)-F12/aug-cc-pVQZ level of theory (Dunning 1998; Raghavachari et al. 1998; Adler et al. 2007; Peterson et al. 2008; Knizia et al. 2009), using the MOLPRO program package (Werner et al. 2020) with only valence electron correlated and then corrected for the basis set superposition error by means of the Boys & Bernardi (1970) counterpoise correction scheme. The formylium structure was held fixed to its experimentally determined equilibrium geometry (Dore et al. 2003), and interaction energies have been computed over a grid of 390 points equally distributed over the $\{R, \theta\}$ Jacobi coordinates, where R is the distance between Ar and the center of mass of HCO^+, while θ is the angle between the HCO^+ molecular axis and the $\boldsymbol{R}$ vector.

Standard time-independent coupled scattering equations were solved using MOLSCAT code (Hutson & Le Sueur 2019). Calculations were carried out at kinetic energy ranging in the 2–500 cm^{-1} interval with narrow steps (1 cm^{-1}) at low energies, gradually increasing up to 50 cm^{-1}. For more details regarding the representation of the potential, employed propagator, the optimization of the rotational basis set parameters and convergence limits, the reader is referred to Tonolo et al. (2021). The pressure-broadening and shift coefficients for the two lowest rotational transitions were derived from the results of the scattering calculations. Specifically, from the S-matrix elements involving both the initial (J) and final ($J + 1$) states of the relevant transition, the $\sigma(E)$ broadening cross sections are derived at each E total energy. The real and imaginary parts of $\sigma(E)$ describe the pressure broadening and shift, respectively, of a given $J + 1 \leftarrow J$ line. These cross sections were then integrated over the entire distribution of the thermal energy

$$\bar{\sigma} = \frac{1}{(kT)^2} \int_0^\infty E e^{-E/kT} \sigma(E) dE, \quad (1)$$

where k is the Boltzmann constant and T is the temperature chosen for the integration, which was set to 98 K to allow for

the comparison with the experimental measurements. The associated pressure-broadening (γ) and pressure-shift (s) coefficients are derived using

$$\gamma - \mathrm{i}s = n_p \bar{\nu}\bar{\sigma} = \frac{2.23627}{\sqrt{\mu T}}\bar{\sigma}, \quad (2)$$

where $\bar{\nu} = (8k_B T/\pi\mu)^{1/2}$ is the mean velocity of the colliders and n_p represents the density of the gas. In terms of units, γ and s are expressed in MHz Torr^{-1}, $\bar{\sigma}$ in Å^2, μ (reduced mass of the system) in u, and T in kelvin.

Ab initio calculations were also employed to derive theoretical estimates of the centrifugal distortion constants of formylium isotopologues. The required anharmonic force fields have been computed using the CCSD(T) method in conjunction with the cc-pCVQZ basis set with all electrons correlated. Second-order vibrational perturbation theory (VPT2) was then applied to derive the quartic (D) and sextic (H) centrifugal distortion constants for $HC^{18}O^+$, $DC^{18}O^+$, $HC^{17}O^+$, and $DC^{17}O^+$.

4. Analysis and Results

4.1. Theoretical Details

The rotational energy of the formylium ion is expressed by a Hamiltonian, which has the form

$$\boldsymbol{H} = \boldsymbol{H}_{\mathrm{rot}} + \boldsymbol{H}_{\mathrm{cd}} + \boldsymbol{H}_{\mathrm{hfs}}, \quad (3)$$

where the first two terms represent the pure rotational energy for a linear molecule corrected for the centrifugal distortion up to the sextic term:

$$\boldsymbol{H}_{\mathrm{rot}} + \boldsymbol{H}_{\mathrm{cd}} = B\boldsymbol{J}^2 - D\boldsymbol{J}^4 + H\boldsymbol{J}^6. \quad (4)$$

The term $\boldsymbol{H}_{\mathrm{hfs}}$ accounts for the hyperfine interaction in the case of $HC^{17}O^+$ due to the spin ($I = 5/2$) of the ^{17}O nucleus (Flygare 1964; Gordy & Cook 1984):

$$\boldsymbol{H}_{\mathrm{hfs}} = e\boldsymbol{Q}\colon \boldsymbol{q} + \boldsymbol{I} \cdot \boldsymbol{C} \cdot \boldsymbol{J}. \quad (5)$$

The first contribution is produced by the nuclear quadrupole coupling and is expressed as dyadic products of the nuclear quadrupole tensor $e\boldsymbol{Q}$, where e is the elementary charge, and the electric field gradient tensor $\boldsymbol{q}$. The second term describes the weak magnetic spin–rotation interaction ($\boldsymbol{C}$ tensor) between the nuclear spin $\boldsymbol{I}$ and the rotation angular momentum $\boldsymbol{J}$. As a result of the interactions described by $\boldsymbol{H}_{\mathrm{hfs}}$, the rotational levels of $HC^{17}O^+$ are split into several (maximum $2I + 1$) sublevels, labeled by the F quantum number values. They correspond to the eigenvalues of the total angular momentum $\boldsymbol{F}$, defined as the vector sum of $\boldsymbol{J}$ and $\boldsymbol{I}$. $\Delta F = 0, \pm 1$ transitions among hyperfine levels give rise to multiplets of hyperfine components, each distributed around the hypothetically unsplit $\Delta J = 1$ pure rotational transition frequency.

4.2. Accurate Determination of the Line Frequencies: Pressure Shift Analysis

Aiming at the determination of very accurate rest frequencies for ionic species, efforts have been taken in order to minimize all possible sources of systematic error, both in the experimental procedure and in the subsequent analysis. The first phenomenon to be considered when measuring the spectra of charged species in the DC glow discharge is the so called "field-drift effect," i.e., the Doppler shift of the line center frequency due to the ion acceleration in the static electric field applied at the electrodes. This is usually appreciable for ions generated in the positive column of the discharge (Sastry et al. 1981) but, for species observed in the negative glow (essentially a field-free region; De Lucia et al. 1983), such a Doppler shift is expected to be very small or negligible. Previous spectroscopic measurements of HCO^+ produced in anomalous discharge conditions (e.g., low current, high DC voltage, coaxial magnetic field applied; see, e.g., Hirao et al. 2007; Tinti et al. 2007) indicated that this ion is indeed produced in the negative column of the plasma and that the field-drift effect does not produce any significant displacement on the retrieved line frequencies.

Another experimental source of systematic error that is worth considering is the pressure shift induced by the collision with the buffer gas. In fact, collisional interactions do not merely cause a broadening of the line profile of a radiative $f \leftarrow i$ transition but also induce a shift of its center position ν_{if}. In scattering theory, this is accounted for by the imaginary part of the corresponding σ_{if} broadening cross section (see Section 3), and the magnitude of the displacement is predicted to have a linear dependence with the pressure of the perturber gas. For neutral species, such a shift is generally very small, and it can be revealed only when highly accurate profile measurements of low-J rotational transitions are performed. On the other hand, in collisional systems involving charged particles, this phenomenon is magnified and accounts for nonnegligible displacements in the measured line positions (see, e.g., Buffa et al. 2006, 2010; Cazzoli et al. 2012; Tonolo et al. 2022). It has to be pointed out that, for ions produced and detected in the plasma, it is not possible to reduce arbitrarily the pressure to minimize the effect, as some amount of buffer gas is required to maintain stable discharge conditions. Ideally, the relevant collision contribution to the measured line positions should be evaluated experimentally.

In the present study, the pressure shift has been determined for the $J = 1 \leftarrow 0$ and $J = 2 \leftarrow 1$ transitions of $HC^{18}O^+$. For these two lines, several spectral recordings were performed at increasing Ar pressure, and the corresponding central frequencies were retrieved using the `proFFiT` line analysis code (Dore 2003). This tool models the spectrum by employing a frequency-modulated, speed-dependent Voigt profile (SDVP; Berman 1972; Pickett 1980) and takes into account the full complex representation of the Fourier-transformed (FT) dipole correlation function. The inclusion of the dispersion term (imaginary part of the FT dipole correlation function) in the analysis provides a direct means of modeling the line asymmetry induced by the parasitic etalon effect of the absorption cell, thus allowing to single out precisely the underlying pressure shift contribution. This implementation of the SDVP function thus has the Lorentzian line half-width (Γ), the quadratic speed-dependent relaxation coefficient (Γ_2), the central frequency (ν), and the dispersion phase factor (ϕ) as adjustable parameters (see Dore 2003 for details).

A subset of the results is illustrated in Figure 1; it shows the experimental and modeled spectral traces for the $J = 1 \leftarrow 0$ and $J = 2 \leftarrow 1$ transitions of $HC^{18}O^+$ recorded at Ar pressure ranging in the 7–22 mTorr interval, all exhibiting flat and featureless residuals. Many series of measurements have been collected in order to improve the statistics. For each spectrum, all the retrieved central frequencies are then plotted against the

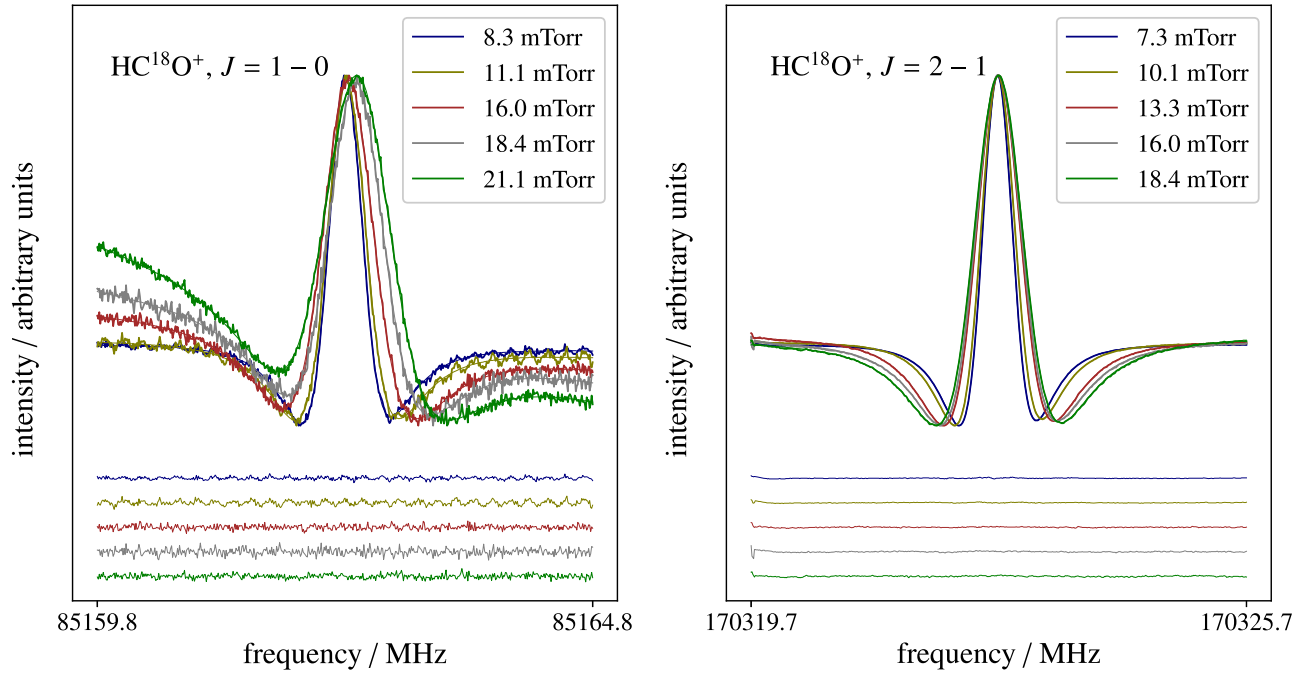

Figure 1. Measured and modeled (SDVP) spectral profiles, together with the corresponding fit residuals, for the $J = 1$–0 (left panel) and $J = 2$–1 (right panel) transitions of $HC^{18}O^+$ for different pressures of the Ar buffer gas.

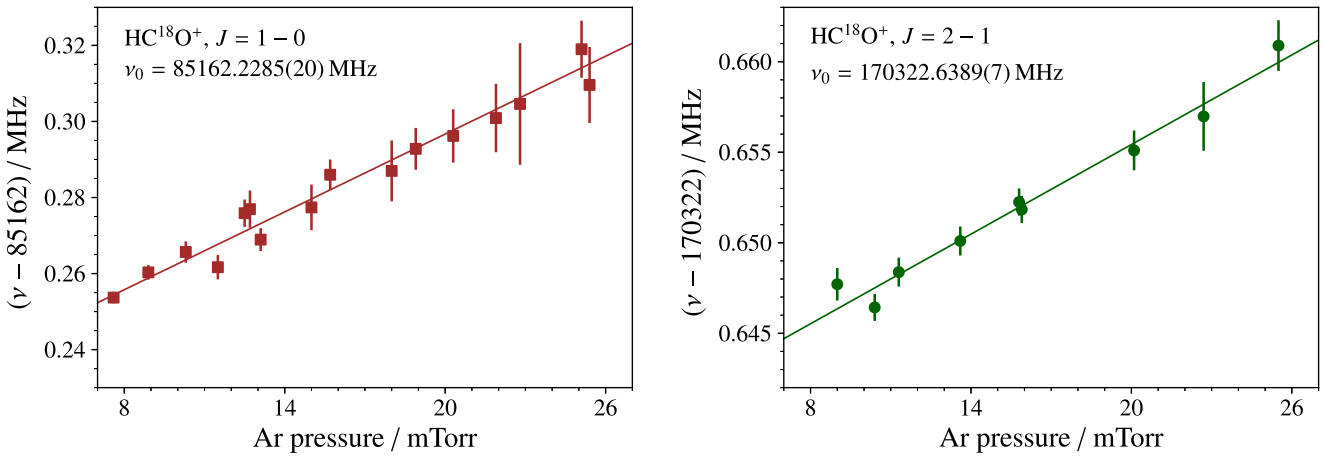

Figure 2. Plot of the retrieved (from SDVP line-profile analysis) central frequency ν for the $J = 1$–0 (left panel) and $J = 2$–1 (right panel) transitions of $HC^{18}O^+$ vs. Ar pressure. The error bars indicate the standard errors of the retrieved line central frequencies. Linear regression (straight trace) has been used to determine the pressure shift coefficients and the corresponding frequencies extrapolated at zero pressure (ν_0).

Ar pressure, as shown in Figure 2, demonstrating the expected linear behavior. Such trends, extrapolated to zero pressure, allow for the derivation of the corresponding "unperturbed" line positions, i.e., purged from the buffer gas collisional contribution. They are $\nu_0(1-0) = 85{,}162.2285(20)$ MHz and $\nu_0(2-1) = 170{,}322.6389(7)$ MHz, respectively. From the analysis, estimates of the pressure broadening γ and shift s coefficients have been also retrieved for both lines; they are collected in Table 1 together with the corresponding theoretically computed values (see Section 3).

Table 1
Experimental Values and Corresponding Theoretical Estimates of the Pressure Broadening (γ) and Shift (s) Coefficients for the $J = 1$–0 and $J = 2$–1 Rotational Transitions of $HC^{18}O^+$

$J' - J$	γ (MHz Torr^{-1})		s (MHz Torr^{-1})	
	Exp.	Theo.[a]	Exp.	Theo.[a]
1–0	20.44(60)	20.513	3.38(18)	2.073
2–1	16.3(13)	17.643	0.826(57)	0.534

Note.
[a] See Section 3 for details.

4.3. Accurate Determination of the Line Frequencies: Unresolved Hyperfine Structure

The rotational spectrum of $HC^{17}O^+$ is peculiar due to the presence of the ^{17}O quadrupolar nucleus ($I = \frac{5}{2}$), which produces an HFS, i.e., the rotational transitions appear as multiplets (see Section 4.1). In general, the patterns consist of widely spaced components for low-J transitions but tend to become narrower as the rotational quantum number increases.

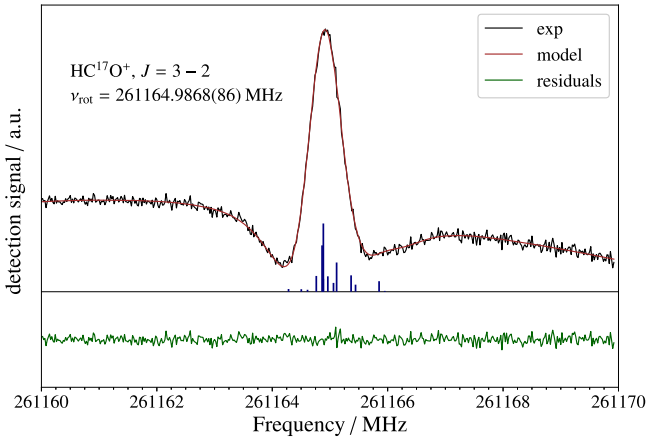

Figure 3. Experimental spectrum, computed profile, and fit residuals for the $J = 3$–2 transition of $HC^{17}O^+$. The spectrum has been modeled as a blend of 14 hyperfine components (blue histogram), each broadened using an SDVP function as described in Section 4.2 with $\Gamma = 0.582(12)$ MHz, $\Gamma_2 = 0.074(15)$ MHz, and $\phi = 2.22(23)°$.

At intermediate-J values, the line profile appears as a broad, often asymmetric feature, produced by the loose overlap of several hyperfine components. In the present experiment, this happens for the $J = 3$–2, $J = 4$–3, and $J = 5$–4 transitions of $HC^{17}O^+$: they do not show a resolvable multiplet but rather a unique, distorted profile. As an example, we show in Figure 3 the recording of the $J = 3$–2 line overlapped with the stick spectrum of the corresponding hyperfine components. This case illustrates that an unresolved, partially collapsed pattern causes some ambiguity when one has to assign the measured line position to a single—or even to a subgroup—of HFS lines.

Using `proFFit`, we modeled the $J = 3$–2, $J = 4$–3, and $J = 5$–4 lines as envelopes of all their hyperfine components (14, 15, and 15, respectively). Each HFS line was modeled using the SDVP function (see Section 4.2) and a common set of profile parameters (i.e., all components shared the same Γ, Γ_2, and ϕ) were then fitted to the experimental spectrum. Frequency splittings and intensities of the HFS multiplets were calculated using the quadrupole coupling and spin rotation constants reported by Dore et al. (2001b) and held fixed, while the central frequency was optimized in the line-profile fit. In this way, one can retrieve from the measurements a hypothetically "unsplit" rotational frequency ν_{rot}, purged from hyperfine contributions to the maximum extent. The analysis yielded $\nu_{rot}(3–2) = 261164.9868(86)$ MHz, $\nu_{rot}(4–3) = 348211.1324(20)$ MHz, and $\nu_{rot}(5–4) = 435249.7064(93)$ MHz, respectively. An illustrative example of this treatment and of the resulting quality of the line-profile modeling are presented in Figure 3.

4.4. Spectral Analysis

Concerning $HC^{18}O^+$, most of the measurements represent new data. For a few low-frequency transitions, earlier laboratory measurements were already available (Plummer et al. 1983; Warner 1988), but we remeasured these lines in order to build up a fully homogeneous data sample. Compared with the new frequencies derived from our spectral recordings, these literature values show deviations ranging in the 6–110 kHz interval. The merged data set of $DC^{18}O^+$ includes seven data from literature: line frequencies from $J = 2$–1 to $J = 8$–7 previously measured by Caselli & Dore (2005). The spectral analysis was performed using the Hamiltonian described by Equation (4) and adjusting the rotational constant B plus the quartic, D, and sextic, H, centrifugal distortion constants. Estimated experimental uncertainties (σ) from 5 to 20 kHz, increasing with frequency, have been assigned to the various measurements for statistical weight evaluation ($w = 1/\sigma^2$). The list of the analyzed experimental frequencies, the resulting spectroscopic parameters, and the correlation matrices for $HC^{18}O^+$ and $DC^{18}O^+$ are collected in Table 2.

The data set of $HC^{17}O^+$ includes the ^{17}O-hyperfine transitions reported in earlier studies (Dore et al. 2001a, 2001b). At the J values sampled by our measurements, no HFS was resolvable. However, each recorded transition was treated in order to recover the profile distortion due to the loosely overlapped multiplets, thus retrieving the corresponding pure rotational frequency (see Section 4.3 for details). Using this approach, we have also remeasured the $J = 3$–2 (from Plummer et al. 1983) and $J = 4$–3 transitions, already reported in Dore et al. (2001b). Experimental uncertainties of 10 kHz or 20 kHz (depending on frequency) have been assigned to our measurements, whereas for the literature data, we retained the original values. Finally, eighteen lines were analyzed using the full Hamiltonian of Equation (3) and fitting all its coefficients, namely, the rotational constant B, the centrifugal distortion parameters D and H, the quadrupole coupling coefficient eQq, and the nuclear spin–rotation interaction constant C. The hyperfine parameters are sensitive only to the low-J data taken from the literature; thus, our determinations essentially coincide with the ones of Dore et al. (2001b). The experimental value, $eQq(^{17}O) = 4.603$ MHz, compares well (<3% discrepancy) with the corresponding computed value of 4.480 MHz obtained at the CCSD(T)/aug-pCVQZ level of theory (see Section 3). To the best of our knowledge, there were no previous laboratory measurements of the rotational spectrum of the $DC^{17}O^+$. In our experiment, we were able to record nine lines for this species. None of them showed a resolvable ^{17}O-quadrupole splitting, though, similarly to what was done for $HC^{17}O^+$; the HFS was considered in the line-profile analysis to improve the accuracy of the retrieved frequency positions. Variable experimental uncertainties ($\sigma = 10$–50 kHz) have been given to these data to take into account the different measurement quality. The spectral analysis of this isotopologue, carried out with Equation (4), yielded the first experimental determination of the rotational constant B and of the quartic (D) and sextic (H) centrifugal distortion constants. The list of the experimental frequencies analyzed for $HC^{17}O^+$ and $DC^{17}O^+$, the resulting spectroscopic constants, and the correlation matrices are gathered in Table 3.

5. Discussion and Conclusions

This work presents a comprehensive laboratory study of the rotational spectra of the ^{18}O- and ^{17}O-containing isotopologues of HCO^+. The spectral recordings have been extended above 1 THz (773 GHz for $DC^{18}O^+$), achieving, for these rare isotopic species, a frequency coverage comparable to that of the parent molecule HCO^+ (e.g., Cazzoli et al. 2012). The analysis yielded very precise values of the rotational constant B and of the quartic centrifugal distortion constant D. As far as $HC^{18}O^+$ and $DC^{17}O^+$ are concerned, our results provided the first set of spectroscopic parameters obtained from extensive laboratory measurements. Similar studies, though more restricted in frequency, had already been carried out for $DC^{18}O^+$(Caselli & Dore 2005) and $HC^{17}O^+$(Dore et al.

Table 2
Results of the Spectral Analyses Performed for $HC^{18}O^+$ and $DC^{18}O^+$

		$HC^{18}O^+$			$DC^{18}O^+$		
J'	J	Observed (MHz)	Obs. − Calc. (kHz)	σ (kHz)	Observed (MHz)	Obs. − Calc. (kHz)	σ (kHz)
1	0	85,162.2285[a]	0.0	5.0	…	…	…
2	1	170,322.6389[a]	−4.7	5.0	137,653.5239[b]	4.0	10.0
3	2	255,479.4336	1.7	10.0	206,477.2402[b]	0.0	5.0
4	3	340,630.7850	4.9	10.0	275,297.3150[b]	2.0	5.0
5	4	425,774.8705	−4.4	10.0	344,112.5213[b]	−1.3	5.0
6	5	510,909.9110	7.3	10.0	412,921.6530[b]	−0.6	5.0
7	6	596,034.0531	−0.3	10.0	481,723.4893[b]	−1.1	5.0
8	7	681,145.5113	−0.5	10.0	550,516.8156[b]	−2.3	10.0
9	8	766,242.4674	0.6	10.0	619,300.4219	1.0	10.0
10	9	851,323.1064	0.1	10.0	688,073.0882	3.1	10.0
11	10	936,385.6214	2.4	10.0	756,833.5979	2.4	10.0
12	11	1,021,428.1925	−1.6	10.0	825,580.7407	2.7	10.0
13	12	1,106,449.0201	−1.1	20.0	894,313.3002	1.3	10.0
14	13	1,191,446.2836	−6.8	20.0	963,030.0618	−2.6	10.0
15	14	1,276,418.1895	−2.9	20.0	1,031,729.8181	−3.7	10.0
17	16	1,361,362.9245	5.8	20.0	1,169,073.4684	7.0	20.0

	rms[c] = 3.8 kHz				rms[c] = 2.9 kHz			
Constant	Value[d]	Correlation matrix			Value[d]	Correlation matrix		
B (MHz)	42,581.26536(23)	1.000			34,413.78525(10)	1.000		
D (kHz)	75.5598(19)	−0.9019	1.000		50.66133(89)	−0.8606	1.000	
H (mHz)	63.3(46)	0.7820	–0.9629	1.000	42.1(21)	0.7434	–0.9655	1.000

Notes. Top frame: analyzed transition frequencies, least-square residuals, and assumed uncertainties. Bottom frame: determined spectroscopic constants, 1σ standard errors, and upper triangles of the corresponding correlation matrices.
[a] Corrected for the pressure shift.
[b] Caselli & Dore (2005).
[c] rms error of the residuals.
[d] Standard errors are reported in parentheses in units of the last quoted digit.

2001a, 2001b); for them, our results show an improvement in precision of a factor of 2 for B and more than 1 order of magnitude for D. The sextic centrifugal distortion constant, H, has also been determined for all four isotopic species with an overall precision of ∼5%, except for $DC^{17}O^+$(∼30%) because of the limited J range sampled by the measurements.

The experimental values of the centrifugal distortion parameters can be compared with the corresponding theoretical estimates. In a comprehensive study, Mladenović (2017) computed (among other quantities) ground-state rotational and centrifugal distortion constants for a number of HCO^+ isotopic variants. This author used a variational approach, involving a global ab initio potential energy surface to derive a large number of rovibrational levels, then empirically fitted to the parameters of a semirigid linear-rotor Hamiltonian (see Mladenović 2017 for details). In this way, theoretical estimates of the ground-state B, D, and H constants were obtained. Conversely, our simpler calculations are based on VPT2 (see Section 4.1) and provided equilibrium values for D and H. Table 4 shows the comparison between these two sets of ab initio computed quantities and the corresponding experimentally derived values.

Concerning D, the theoretical ground-state estimates of Mladenović (2017) are placed almost exactly at the middle between our ab initio equilibrium value and the corresponding experimental finding, with all computed values being underestimated. This seems to indicate that their sophisticated approach yields more accurate predictions than our VPT2-based ones (∼1% versus 2%–3%), but it is still unable to fully recover the zero-point vibrational contribution. Generally speaking, the sextic centrifugal distortion constant, H, is an intrinsically "weak" parameter: when empirically derived, it is subject to large deviations in response to minor systematic measurement errors. Hence, the theoretical calculations serve primarily to asses a posteriori the reliability of the spectral analysis results. In this respect, for $HC^{18}O^+$ and $DC^{18}O^+$, there is an almost perfect match between the experimental values and the ones computed by Mladenović (2017). On the other hand, the agreement is only moderate for ^{17}O-bearing isotopologues, with $HC^{17}O^+$ showing the largest departure ($H^{exp}/H^{theor} \sim 2$). Most likely, the discrepancy for this species is attributable to its peculiar spectral analysis, in which a partially resolved HFS (Dore et al. 2001b) has been fitted together with a subset of hypothetically "pure" rotational frequencies (for $J > 2$). Here, any minor inaccuracy in the modeling of the hyperfine contributions at low J is capable to slightly alter the centrifugal trend caught by the J^6 coefficient. In fact, removing all the HFS components from the fits, one gets $H = 85(18)$ mHz, a value in agreement with the corresponding theoretical prediction.

As a general remark, moving to the experimental fits, we point out that the agreement between experimental and computed frequencies is remarkable. For $HC^{18}O^+$ and $DC^{18}O^+$, whose recordings are characterized by a large signal-to-noise ratio and where the line profiles are not

Table 3
Results of the Spectral Analyses Performed for $HC^{17}O^+$ and $DC^{17}O^+$

				$HC^{17}O^+$			$DC^{17}O^+$		
J'	F'	J	F	Observed (MHz)	Obs. − Calc. (kHz)	σ (kHz)	Observed (MHz)	Obs. − Calc. (kHz)	σ (kHz)
1	1.5	0	2.5	87,056.9660[a]	11.4	10.0	⋯	⋯	⋯
1	3.5	0	2.5	87,057.2580[a]	19.8	10.0	⋯	⋯	⋯
1	2.5	0	2.5	87,058.2940[a]	13.1	10.0	⋯	⋯	⋯
2	1.5	1	2.5	174,112.1760[a]	−7.4	20.0	⋯	⋯	⋯
2	2.5	1	2.5	174,112.9456[a]	19.2	20.0	⋯	⋯	⋯
2	0.5	1	1.5	⋯	⋯	⋯	⋯	⋯	⋯
2	3.5	1	2.5	⋯	⋯	⋯	⋯	⋯	⋯
2	4.5	1	3.5	⋯	⋯	⋯	⋯	⋯	⋯
2	1.5	1	1.5	174,113.5290[a]	19.2	20.0	⋯	⋯	⋯
2	2.5	1	3.5	174,114.0183[a]	−1.6	20.0	⋯	⋯	⋯
2	3.5	1	3.5	⋯	⋯	⋯	⋯	⋯	⋯
2	2.5	1	1.5	⋯	⋯	⋯	⋯	⋯	⋯
3	⋯	2	⋯	261,164.9868	−2.0	10.0	211,019.477	−18.9	20.0
4	⋯	3	⋯	348,211.1324	−10.4	10.0	281,353.390	3.7	10.0
5	⋯	4	⋯	435,249.7064	−11.9	10.0	351,682.177	−8.0	10.0
6	⋯	5	⋯	522,278.8233	−2.0	10.0	422,004.631	9.7	10.0
7	⋯	6	⋯	609,296.5643	6.1	10.0	492,319.427	1.9	10.0
8	⋯	7	⋯	696,301.0311	−4.8	10.0	562,625.315	−12.8	20.0
9	⋯	8	⋯	783,290.3748	12.4	20.0	632,921.010	−52.6	50.0
10	⋯	9	⋯	870,262.6556	9.8	20.0	703,205.381	16.3	50.0
11	⋯	10	⋯	957,215.9942	−1.0	20.0	773,476.983	12.1	50.0
12	⋯	11	⋯	1,044,148.5121	−8.7	20.0	⋯	⋯	⋯
13	⋯	12	⋯	1,131,058.3363	2.6	20.0	⋯	⋯	⋯

	$HC^{17}O^+$ rms[b] = 10.0 kHz						$DC^{17}O^+$ rms[b] = 20.8 kHz				
Constant	Value[c]	Correlation matrix					Value[c]	Correlation matrix			
B (MHz)	43,528.91928(87)	1.000					35170.8710(13)	1.000			
D (kHz)	78.953(11)	−0.909	1.000				53.063(25)	−0.945	1.000		
H (mHz)	124.4(42)	0.819	–0.974	1.000			32(13)	1.000	0.839	–0.956	1.000
eQq (MHz)	4.603(39)	−0.021	0.018	–0.016	1.000		⋯	⋯			
C (kHz)	−21.7(21)	0.173	–0.154	0.138	–0.262	1.000	⋯	⋯			

Notes. Top frame: analyzed transition frequencies, least-square residuals, and assumed uncertainties. Bottom frame: determined spectroscopic constants, 1σ standard errors, and upper triangles of the corresponding correlation matrices.
[a] Taken from Dore et al. (2001b).
[b] rms error of the residuals.
[c] Standard errors are reported in parentheses in units of the last quoted digit.

complicated by the presence of an underlying HFS, the fit residuals do not exceed 10 kHz, with an average accuracy better than one part in 10^9 over the sampled frequency interval. Crucial, in this respect, is the correction of the pressure shift, capable of displacing significantly the center frequencies of the low-J transition of ionic species. Inspection of Table 1 shows that our measurements reliably accounted for such a collisional effect. Both the experimentally derived broadening (γ) and shift (s) coefficients compare well with their theoretical estimates. In particular, for both transitions, the shift parameter s agrees both in sign and in the order of magnitude (30%–50%) with their corresponding ab initio value.

The discussion of the previous sections highlights the extra precision achieved by the resulting spectroscopic constants that can be used to effectively update the entries 031506, 032505, and 030505 in the Cologne Database for Molecular Spectroscopy (CDMS; Müller et al. 2005; Endres et al. 2016). No previous spectral predictions were instead available for $DC^{17}O^+$. Prior to this work, the shortage of laboratory data limited the precision and accuracy of the rest-frequency compilations of heavy-O-bearing isotopologues of formylium, especially at high-J values. For example, in the THz regime, the present CDMS entry for the $J = 13$–12 line of $HC^{18}O^+$ has a 1σ uncertainty of ∼2.2 MHz. The same transition computed from our results is ∼2.4 MHz apart and has a prediction error of ∼2.5 kHz, which translates to 1σ radial equivalent velocity error of 0.6 m s^{-1}.

Even at lower-J values, the impact of inaccurate rest frequencies on the astrophysical application can be significant. For example, in a recent paper, Furuya et al. (2022) presented an Atacama Large Millimeter/submillimeter Array study of the $HC^{18}O^+$ distribution in the TW Hya protoplanetary disk. These authors used a rest frequency for the $HC^{18}O^+$ $J = 4$–3 line of 340,632.9780 MHz, whereas from our laboratory data analysis, one gets 340,630.7800(14) MHz. This ∼2.2 MHz discrepancy translates into a 1.94 km s^{-1} velocity error that clearly affects the resulting weighted mean velocity map shown in their Figure 1.

Table 4
Comparison between Experimentally Derived and Theoretically Computed Quartic and Sextic Centrifugal Distortion Constants

Species/ Parameter		Experiments	Theory[a] (Literature)	Theory[b] (This Work)
$HC^{18}O^+$				
	D (kHz)	75.5598(19)	74.76	74.02
	H (mHz)	63.3(46)	61	51.0
$DC^{18}O^+$				
	D (kHz)	50.66133(89)	50.13	49.16
	H (mHz)	42.1(21)	43	32.8
$HC^{17}O^+$				
	D (kHz)	78.953(11)	78.10	77.31
	H (mHz)	124.4(42)	65	54.7
$DC^{17}O^+$				
	D (kHz)	53.063(25)	52.49	51.47
	H (mHz)	32(13)	46	35.0

Notes.
[a] Ground-state values from Mladenović (2017).
[b] Equilibrium values computed as described Section 3.

Acknowledgments

This work has been supported by MIUR (PRIN grant No. 202082CE3T) and the University of Bologna (RFO funds). The COST Action CA21101 "COSY-Confined molecular systems: from a new generation of materials to the stars" is also acknowledged.

ORCID iDs

Luca Bizzocchi https://orcid.org/0000-0002-9953-8593
Francesca Tonolo https://orcid.org/0000-0002-9555-7834
Paola Caselli https://orcid.org/0000-0003-1481-7911
Mattia Melosso https://orcid.org/0000-0002-6492-5921
Luca Dore https://orcid.org/0000-0002-1009-7286
Silvia Alessandrini https://orcid.org/0000-0003-3152-3261
Cristina Puzzarini https://orcid.org/0000-0002-2395-8532
Andrea Pietropolli Charmet https://orcid.org/0000-0002-1490-5754

References

Adler, T. B., Knizia, G., & Werner, H.-J. 2007, JChPh, 127, 221106
Agúndez, M., & Cernicharo, J. 2006, ApJ, 650, 374
Berman, P. R. 1972, JQSRT, 12, 1331
Bizzocchi, L., Lattanzi, V., Laas, J., et al. 2017, A&A, 602, A34
Botschwina, P., Horn, M., Flügge, J., & Seeger, S. 1993, J. Chem. Soc., Faraday Trans., 89, 2219
Boys, S. F., & Bernardi, F. 1970, MolPh, 19, 553
Buffa, G., Dore, L., Tinti, F., & Meuwly, M. 2006, Chem. Phys. Chem., 7, 1764
Buffa, G., Tarrini, O., Dore, L., & Meuwly, M. 2010, Chem. Phys. Chem., 14, 3141
Buhl, D., & Snyder, L. E. 1970, Natur, 228, 267
Caselli, P., & Dore, L. 2005, A&A, 433, 1145
Caselli, P., Walmsley, C. M., Zucconi, A., et al. 2002, ApJ, 565, 331
Cazzoli, G., Cludi, L., Buffa, G., & Puzzarini, C. 2012, ApJS, 203, 11
Cazzoli, G., Puzzarini, C., & Lapinov, A. V. 2003, ApJL, 592, L95
Cazzoli, G., Puzzarini, C., & Lapinov, A. V. 2004, ApJ, 611, 615
De Lucia, F. C., Herbst, E., Plummer, G. M., & Blake, G. A. 1983, JChPh, 78, 2312
Dore, L. 2003, JMoSp, 221, 93
Dore, L., Beninati, S., Puzzarini, C., & Cazzoli, G. 2003, JChPh, 118, 7857
Dore, L., Cazzoli, G., & Caselli, P. 2001a, A&A, 368, 712
Dore, L., Puzzarini, C., & Cazzoli, G. 2001b, CaJPh, 79, 359
Dunning, T. H., Jr 1998, JChPh, 90, 1007
Endres, C. P., Schlemmer, S., Schilke, P., Stutzki, J., & Müller, H. S. P. 2016, JMoSp, 327, 95
Ferrer Asensio, J., Spezzano, S., Caselli, P., et al. 2022, A&A, 667, A119
Flygare, W. H. 1964, JChPh, 41, 793
Furuya, K., Tsukagoshi, T., Qi, C., et al. 2022, ApJ, 926, 148
Gordy, W., & Cook, R. L. 1984, Microwave Molecular Spectra (New York: Wiley)
Herbst, E., & Klemperer, W. 1974, ApJ, 188, 255
Hirao, T., Yu, S., & Amano, T. 2007, JChPh, 127, 074301
Hutson, J. M., & Le Sueur, C. R. 2019, CoPhC, 241, 9
Knizia, G., Adler, T. B., & Werner, H.-J. 2009, JChPh, 130, 054104
Lattanzi, V., Walters, A., Drouin, B. J., & Pearson, J. C. 2007, ApJ, 662, 771
Milam, S. N., Savage, C., Ziurys, L. M., & Wyckoff, S. 2004, ApJ, 615, 1054
Mladenović, M. 2017, JChPh, 147, 114111
Müller, H. S. P., Schlöder, F., Stutzki, J., & Winnewisser, G. 2005, JMoSt, 742, 215
Peterson, K. A., Adler, T. B., & Werner, H.-J. 2008, JChPh, 128, 084102
Pickett, H. M. 1980, JChPh, 73, 6090
Plummer, G. M., Herbst, E., & De Lucia, F. C. 1983, ApJ, 270, L99
Puzzarini, C., Tarroni, R., Palmieri, P., Carter, S., & Dore, L. 1996, MolPh, 87, 879
Qi, C., Kessler, J. E., Koerner, D. W., Sargent, A. I., & Blake, G. A. 2003, ApJ, 597, 986
Raghavachari, K., Trucks, G. W., Pople, J. A., & Head-Gordon, M. 1998, CPL, 157, 479
Riechers, D. A., Weiß, A., Walter, F., & Wagg, J. 2010, ApJ, 725, 1032
Sastry, K. V. L. N., Herbst, E., & de Lucia, F. C. 1981, JChPh, 75, 4169
Schmid-Burgk, J., Muders, D., Müller, H. S. P., & Brupbacher-Gatehouse, B. 2004, A&A, 419, 949
Tafalla, M., Mardones, D., Myers, P. C., et al. 1998, ApJ, 504, 900
Tinti, F., Bizzocchi, L., Degli Esposti, C., & Dore, L. 2007, ApJ, 669, L113
Tonolo, F., Bizzocchi, L., Melosso, M., et al. 2021, JChPh, 155, 234306
Tonolo, F., Lique, F., Melosso, M., Puzzarini, C., & Bizzocchi, L. 2022, MNRAS, 516, 2653
Warner, H. W. 1988, PhD thesis, Univ. of Wisconsin-Madison
Werner, H.-J., Knowles, P. J., Manby, F. R., et al. 2020, JChPh, 152, 144107
Woods, R. C., Dixon, T. A., Saykally, R. J., & Szanto, P. G. 1975, PhRvL, 35, 1269